J. Fluid Mech. (1993), *vol.* 252, *pp.* 173–186

A field experiment on the mechanics of irregular gravity waves

By P. BOCCOTTI, G. BARBARO AND L. MANNINO

Department of Fluid Mechanics and Offshore Engineering, University of Reggio Calabria, Via E. Cuzzocrea, 48, 89100 Reggio Calabria, Italy

(Received 27 March 1991 and in revised form 4 January 1993)

In random wind-generated wave motion on the sea surface, extreme wave events have been shown theoretically to occur within groups with a well-defined configuration and time history that can be specified in terms of the space–time autocovariances of the surface displacement. The predictions of the theory have been tested in a field experiment in the Straits of Messina in which an array of nine wave gauges and nine pressure transducers supported by vertical piles provided space–time information on waves generated over a fetch of approximately 10 km. It was confirmed that the general configuration of the extreme wave groups measured was consistent with the theoretical predictions in terms of the measured space–time autocovariance. During the development stage of a group, as the height of the central (outstanding) wave grows to a maximum, the width of the wave front reduces to a minimum. As an individual wave passes through the group, its wavelength decreases as the wave height increases towards the apex, after which the wavelength increases again as the wave moves towards the front of the group and abates.

1. Introduction

When an extremely high individual wave occurs in a random wind-generated sea state, assumed Gaussian, the expected or average configuration surrounding the high wave crest has been shown (Boccotti 1988, 1989) to be specified in terms of the autocovariance of the random wave field,

$$\Psi(\boldsymbol{X}, T) = \langle \eta(\boldsymbol{x}, t)\, \eta(\boldsymbol{x}+\boldsymbol{X}, t+T) \rangle, \tag{1.1}$$

where $\eta(\boldsymbol{x}, t)$ is the surface displacement. Specifically, if the extreme wave crest occurs at $\boldsymbol{x}_0 = (x_0, y_0)$ at time t_0, with a crest-to-trough height of H, the mean surface configuration in space and time is given by

$$\eta_G(\boldsymbol{x}_0+\boldsymbol{X}, t_0+T) = \frac{H}{2}\left\{\frac{\Psi(\boldsymbol{X}, T) - \Psi(\boldsymbol{X}, T-T^*)}{\Psi(\boldsymbol{0}, 0) - \Psi(\boldsymbol{0}, T^*)}\right\}, \tag{1.2}$$

where T^* is the abscissa of the absolute minimum of the autocovariance function, which is assumed to exist and to be the first minimum after $T = 0$. The result (1.2) assumes that H is very large compared with the mean wave height, or with $\sigma = (\overline{\eta^2})^{\frac{1}{2}}$ for the wave field as a whole and, in effect, that the spectrum is narrow in the sense described by Longuet-Higgins (1984), so that Ψ is a damped oscillatory function in $\boldsymbol{X}$ and T. Superimposed on the deterministic form (1.2) is of course the 'random noise' of the residual wave field whose r.m.s. surface displacement approaches σ as $\boldsymbol{X}$ and T

increase, but when H/σ is large, the variations in the actual sea surface configuration about η_G near the crest are small compared with η_G itself.

Associated with the configuration (1.2) is a distribution of velocity potential in the water, which to the lowest order in a Stokes expansion is given by

$$\phi_G(\boldsymbol{x}_0+\boldsymbol{X}, z, t_0+T) = \frac{H}{2}\left\{\frac{\Phi(\boldsymbol{X}, z, T)-\Phi(\boldsymbol{X}, z, T-T^*)}{\Psi(\boldsymbol{0}, 0)-\Psi(\boldsymbol{0}, T^*)}\right\}, \tag{1.3}$$

where

$$\Phi(\boldsymbol{X}, z, T) = \langle \eta(\boldsymbol{x}, t)\,\phi(\boldsymbol{x}+\boldsymbol{X}, z, t+T)\rangle. \tag{1.4}$$

Note that the hypothesis that H/σ is large is not necessarily inconsistent with the use of the lowest-order (linear) terms in the Stokes expansion, provided H remains small with respect to the wavelength and the water depth. In nature, the very highest waves may be spilling, or almost breaking near the crests and this will produce a localized profile distortion, but the overall configuration should be close to that specified by (1.2). Note also that if η and ϕ are taken as solutions to the linear problem, then so are η_G and ϕ_G, since these are defined as local averages of η and ϕ. This can also be demonstrated formally from (1.2) and (1.3).

The detailed profile (1.2) and velocity potential distribution (1.3) depend on the forms of the autocorrelation functions, or equivalently, of the two-dimensional wave spectrum. Usually, the expected free-surface elevation has the configuration of a wave group with a central very high wave crest passing $\boldsymbol{x}_0$ at time t_0, and its distribution in space and evolution in time is prescribed by expression (1.2). For example, suppose the directional frequency spectrum, defined so that

$$\int_{-\pi}^{\pi}\int_0^{\infty} S(\omega, \theta)\,\mathrm{d}\omega\,\mathrm{d}\theta = \overline{\eta^2},$$

is taken as that used by Hasselmann *et al.* (1973) with the spreading function of Mitsuyasu *et al.* (1975). In deep water, this has the form

$$\left.\begin{aligned} &S(\omega, \theta) = \alpha g^2\omega^{-5}\exp\left[-\frac{5}{4}\left(\frac{\omega_d}{\omega}\right)^4\right]\exp\left\{\ln(\gamma)\exp\left[-\frac{(\omega-\omega_d)^2}{2\chi^2\omega_d^2}\right]\right\} N(n)\,|\cos\tfrac{1}{2}(\theta-\theta_0)|^{2n}, \\ &n = n_0\left(\frac{\omega}{\omega_d}\right)^5 \quad \text{if} \quad \omega \leqslant \omega_d, \quad n = n_0\left(\frac{\omega}{\omega_d}\right)^{-2.5} \quad \text{if} \quad \omega > \omega_d, \quad N(n) = \left[\int_{-\pi}^{\pi}\cos^{2n}\tfrac{1}{2}\theta\,\mathrm{d}\theta\right]^{-1}, \end{aligned}\right\} \tag{1.5}$$

where the parameters γ, χ and n_0 are taken respectively as 3, 0.08 and 20, as Hasselmann *et al.* and Mitsuyasu *et al.* suggest. The covariance functions in (1.2) can be expressed in terms of the spectra; for example

$$\Psi(\boldsymbol{X}, T) = \int_{-\pi}^{\pi}\int_0^{\infty} S(\omega, \theta)\cos(\boldsymbol{k}\cdot\boldsymbol{X}-\omega T)\,\mathrm{d}\omega\,\mathrm{d}\theta, \tag{1.6}$$

where

$$\boldsymbol{k}\cdot\boldsymbol{X} = \frac{\omega^2}{g}(X\sin\theta + Y\cos\theta).$$

The substitution of (1.6) into (1.2) gives η_G as a function of position and time surrounding $\boldsymbol{X} = 0$, $T = 0$, and leads to the sequence of configurations illustrated in figure 1, representing a wave group moving along the y-axis, the dominant direction of the spectrum.

The basic phenomena that occur during the course of evolution of the group are not

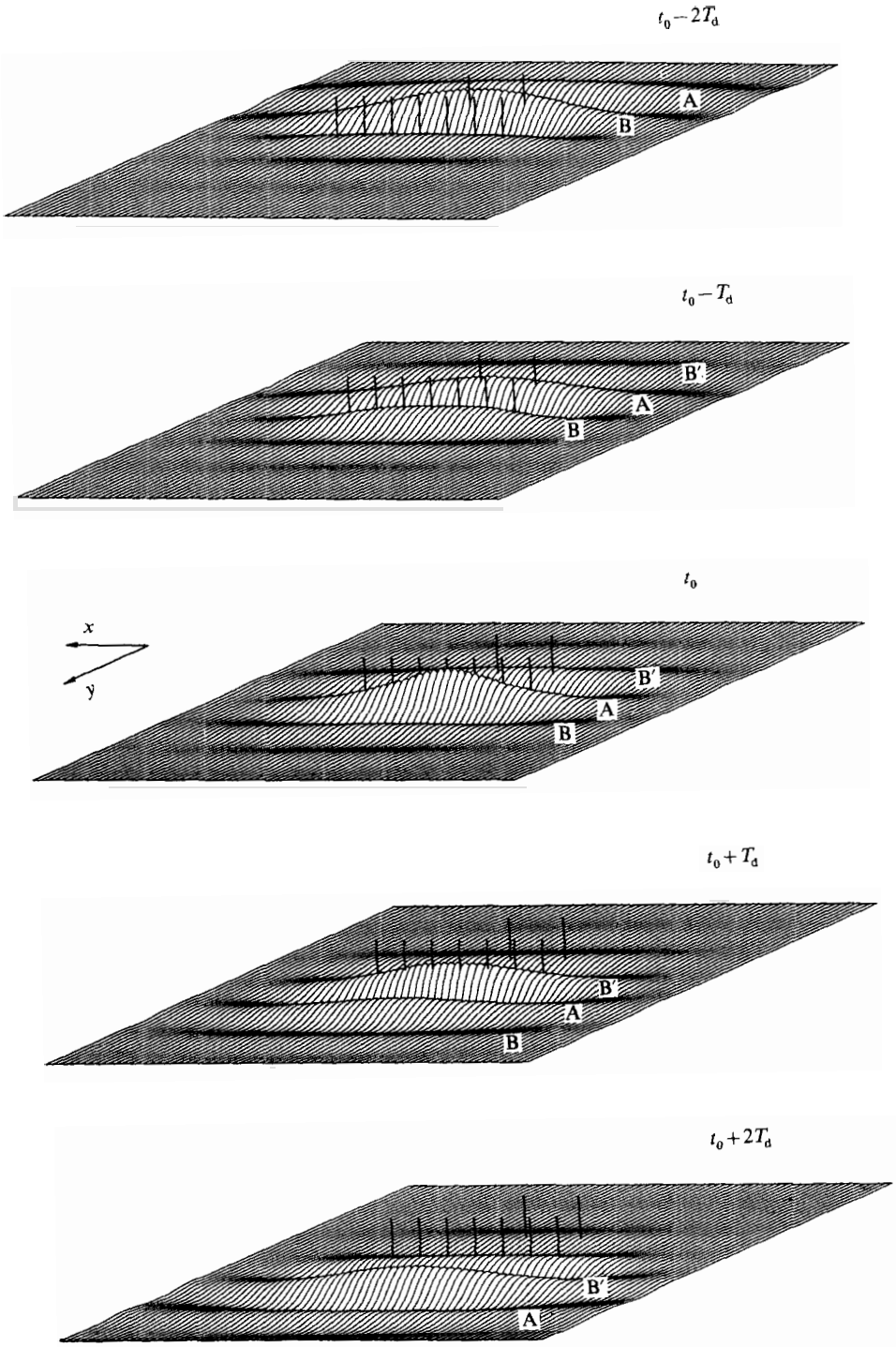

FIGURE 1. Quasi-determinism of the extreme wave events in a random wind-generated sea state, assumed Gaussian, (Boccotti 1989): an extremely high individual wave at a point x_0, y_0 (centre of the framed area), with a probability approaching 1, is produced by the transit of the wave group shown by the pictures. The water is deep; the spectrum of the sea state is that described in §1. The time interval between two consecutive pictures is equal to one wave period T_d and the area shown is 3 wavelengths L_d along the x-axis and $6L_d$ along the y-axis.

dependent on the detailed shape of the wave spectra, though the shape of the group does vary somewhat. If the directional spread of the spectrum increases, the wave front narrows, as illustrated by Boccotti (1988, 1989) while if the spectrum is extended over a wider frequency range, the group envelope becomes shorter in the direction of propagation. Three important characteristics are, however, preserved.

First, the wave group representing the expected configuration of the surface has a development stage in which the height of the central wave grows to a maximum and the width of the wave front reduces to a minimum. The slope along the crest of the central wave then rises to a maximum at the apex of its development and afterwards subsides. Secondly, the individual waves have a propagation speed greater than the envelope (which advances at a speed close to the group velocity). Each wave crest is born at the tail of the group, grows to a maximum when it reaches the central position and then dies at the head of the group, as illustrated by wave A in figure 1. Finally, it is found that as an individual wave approaches the central position of the group, its wave period and wavelength reduce somewhat, attaining a minimum at the apex of the group. As it leaves the central position, a compensating stretching occurs.

In summary, the occurrence of an individual wave height H that is very large compared with the mean can be associated with the centre of a well-defined wave group at the apex of its development, whose configuration and evolution can be predicted in terms of the space–time autocovariance of the wave field as a whole.

2. The field experiment

In order to test the predictions described above, a small-scale field experiment was undertaken during May 1990 at a location off the beach at Reggio Calabria on the eastern coast of the Straits of Messina. Figure 2 shows the site of the experiment. The winds in the area often remain constant from the North West for several consecutive days. After two days of NW wind, the southerly swells usually vanish and the sea state in front of Reggio Calabria city consists of pure wind waves with a significant height typically between 0.2 and 0.4 m and peak period between 2.0 and 2.5 s.

An array of nine small towers was installed 20 m from the beach in the configuration shown in figure 3. These rested on the sea bed, their bases (0.8 m square) being ballasted by pig iron disks and the whole assembly being stiffened by four iron cables between the base and the tower. The inner row (numbered 1–7) were in 3 m of water and the outer pair (8, 9) in 4 m, so that as far as propagation of 2.5 s waves is concerned, the water was in effect deep.

Each tower had at the top on one side an ultrasonic wave probe, from the Delft Hydraulics Laboratory, having a range 0.6–2.0 m, and on the other side a capacitance wave staff with range 0–1.2 m. A pressure transducer (full scale 0.175 bar) was fixed to a short horizontal beam, some 0.5 m below the water surface, which could be turned by divers to bring the pressure transducer onto the same vertical line as the ultrasonic probe or the capacitance wave staff. During the experiment, the average depth of the transducer was 0.53 m with a variation of 0.08 m resulting from the tide. The gauge facilities were completed by a directional current meter supported by one of the piles, whose function was to ensure that the current effects were negligible for the waves: if the current speed exceeded 5% of the phase velocity, the experiment had to be interrupted. The wave gauges and the pressure transducers were connected by submarine cables to an A/D converter unit in an onshore building. The sampling rate was 10 Hz for each gauge and the data were stored in two personal computers. Since the station was equipped to receive data (wave elevation and pressure) from eight

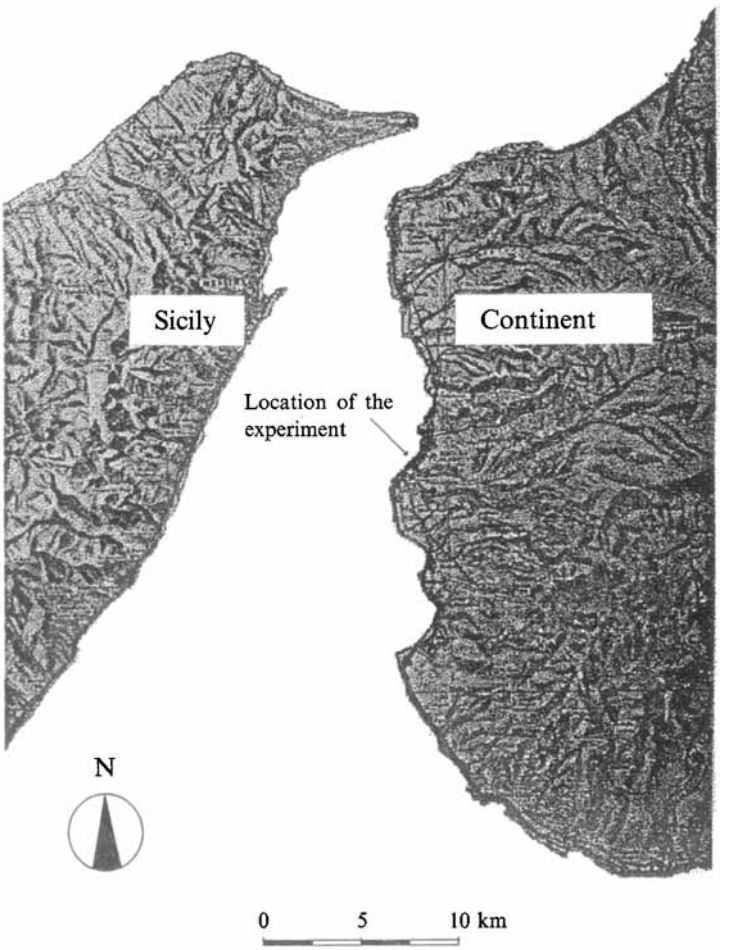

FIGURE 2. The experiment was executed off the beach at Reggio Calabria.

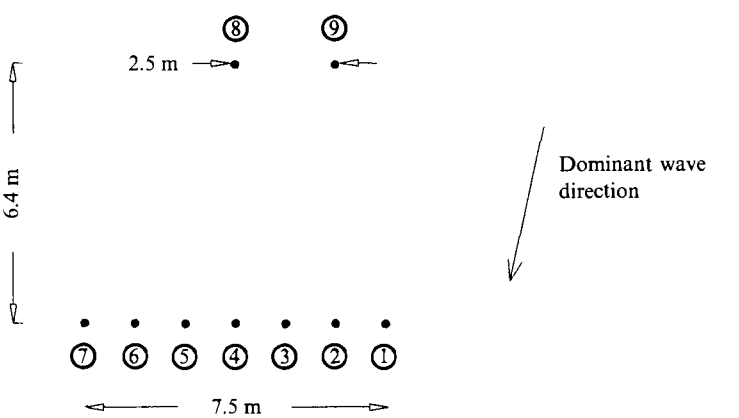

FIGURE 3. Plan view of the small towers which supported the gauges. The configuration of the towers is also shown in figure 1 where the dominant wavelength L_d is assumed to be 7.5 m.

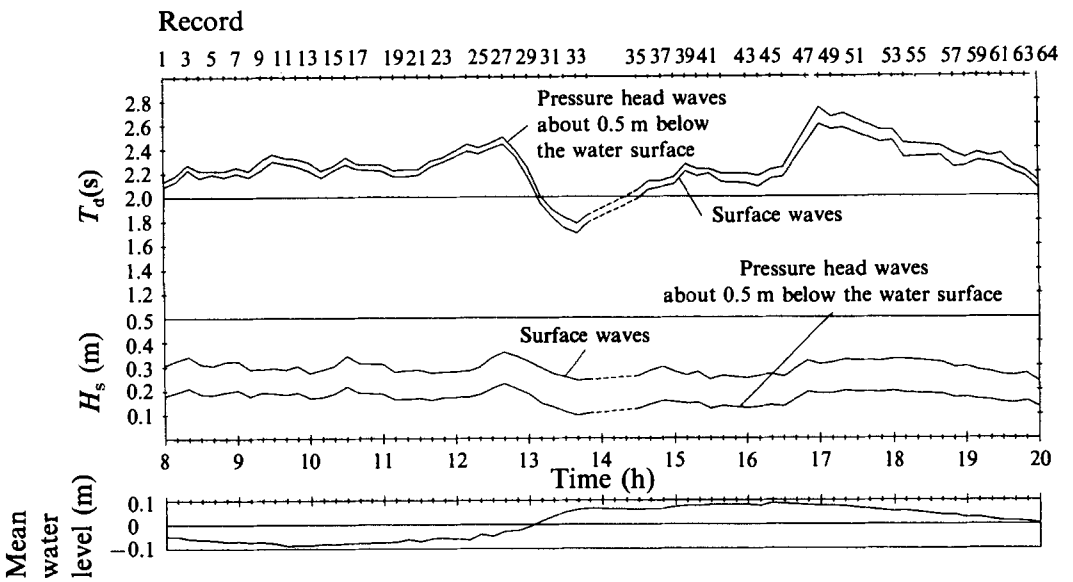

FIGURE 4. Time histories of the significant wave height H_s, of the dominant wave period T_d and of the mean water level during the 12 hours of the experiment (at water level 0, the depth of the transducers was 0.53 m).

towers only, one of the nine had to be disconnected. During the experiment, tower six was disconnected because its ultrasonic probe was damaged.

In a series of preliminary trials, the gain of a few capacitance-type staffs presented some fluctuations which were identified by intercomparison among the wave staffs and with the pressure transducers. There also seemed to be some departures from linearity in these capacitance staffs. The ultrasonic probes, on the other hand, did not present any of these defects, and so were selected for the final experiment. The only defect that we detected was an occasional drop-out of the reflected ultrasonic beam for short time intervals. In those intervals, the gauge's output maintained the last correctly measured values.

Suitable wind and wave conditions with a steady wind of about 7 m/s over a fetch of 10 km and the absence of southerly swell, were encountered ten days after the array was installed. The experiment was conducted over a 12 hour period, starting at 8 am on May 10, 1990. A total of 64 records was obtained, each of nine minutes duration and containing 280 to 360 dominant waves. Measurements were suspended between 2 and 3 pm because the current was too large and some additional short interruptions occurred for data copying operations.

The time histories of the significant wave height H_s (being defined as 4σ) and of the dominant wave period T_d are shown in figure 4. T_d is defined here as the average zero up-crossing period of the two highest waves of the autocovariance function. It is very close to the peak period of a narrow spectrum and its evaluation from a time series is not affected by uncertainty. The values of significant wave height H_s and peak period T_d are the averages of the eight measurements by ultrasonic probes for the surface waves, and of the eight measurements by transducers for the pressure head waves. These reveal, at first glance, good consistency between the measurements of the ultrasonic probes and those of the pressure transducers – each growing or decaying trend recorded by one of the gauges is also revealed by the other. Clearly, the height of the pressure head waves is smaller than that of the surface waves, as consequence

of the attenuation with depth (see the Appendix). Moreover, since the attenuation is more intense for the waves with the shorter periods, the dominant period is somewhat greater in the pressure head waves than in the surface waves. Figure 4 also shows the mean water level during the 12 hours of the experiment, which proved to be practically the same whether evaluated from the ultrasonic probes or from the pressure transducers.

Individual wave heights and periods were obtained in two ways. Selection of the highest waves was made both with a zero up-crossing definition (a wave consisting of a crest and the following trough) and with a zero down-crossing definition (a trough and the following crest). The greatest wave heights H in each of the 64 records ranged from 9.66σ to 6.82σ, or about 2.5 to 1.7 times the significant wave height. The total number of waves passing the array was nearly 20000, but the number of waves considered in order to identify the maxima was sixteen times larger, because of the eight measurement points and the two definitions. Figure 5 shows the measured frequency of occurrence of wave heights for zero up-crossings as a function of H/σ. The line represents the classic Rayleigh expression $P = \exp(-H^2/8\sigma^2)$, which, as usual, overestimates by a few percent the wave heights in the range of the largest H/σ values (Longuet-Higgins 1980; Forristall 1984).

3. Results of the experiment

3.1. *Expected extreme wave characteristics*

The space–time covariances in equations (1.2) and (1.3) can be found from the measurements by cross-correlation of the time series obtained at the discrete measurement locations, and if an extreme wave is encountered at one such location, the time history of the expected surface configuration at this, and the other locations, can be calculated from (1.2). Similarly, the variations in pressure at a fixed depth are given by $-\rho\partial\phi/\partial t$ or $\rho g\zeta$ where ζ is the fluctuating 'pressure head' at this depth, so that the derivative of (1.3) with respect to T provides a corresponding relation between the expected pressure variation at a fixed depth below an extreme wave and the pressure–surface displacement covariances of the whole record.

The highest wave (as a multiple of σ) in the whole experiment was a zero down-crossing recorded by gauge 3 during record 24. With (x_0, y_0) taken as the location of this gauge and t_0 the instant at which this wave passed, the vectors $\boldsymbol{X}$ are specified by the relative locations of the other gauges. The time series data of record 24 provided measured autocovariances as a function of T for the various gauge locations and these were used, without smoothing, on the right-hand side of (1.2) to estimate $\eta(t_0+T)$ at these locations in an extreme wave. (The sign was reversed because of the zero down-crossing definition.) The results are shown in figure 6.

In this figure, A denotes the wave which is highest at location 3, and B is the wave immediately *before* this one. Note that at locations 8, 9, wave B is slightly larger than A, but as it passes to the line 1–7, it decreases, passing from the centre to the head of the group while the succeeding wave A grows because it replaces B at the group centre. Note also that the period of wave B increases as it passes from the centre to the head of the group while the period of wave A decreases as it reaches its maximum height. The direction of the wave can be estimated accurately since the front of wave A in the central position of the group along the traverse of locations 1–7 proves to be nearly straight. The relative phases indicated an angle of incidence of 11° – the front centre transits point 9 before point 3, and this is consistent with the fact that in figure 6, the wave group at point 9 is higher than at point 8.

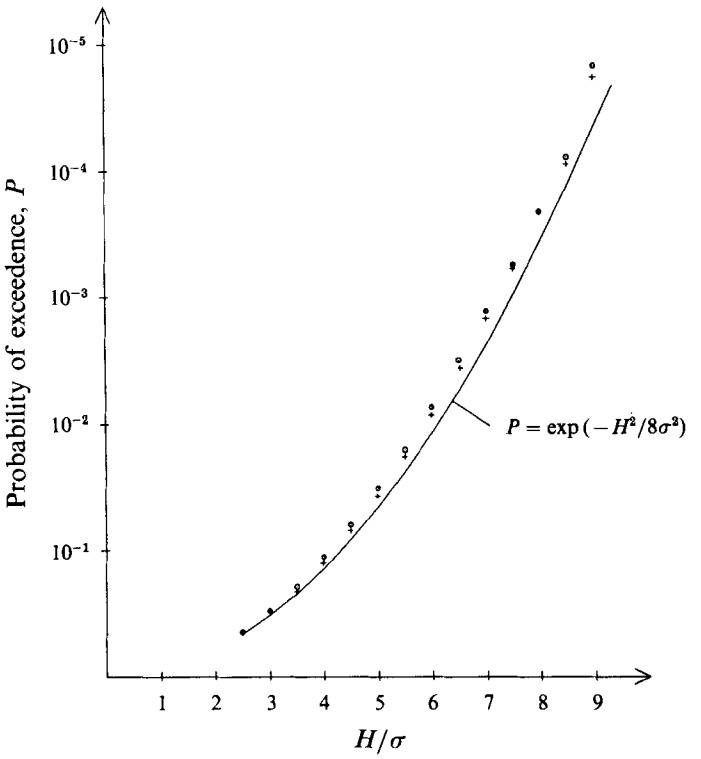

FIGURE 5. Probability that a wave has a height greater than a given value: ○, surface waves; +, pressure head waves.

Similar calculations have been performed for all the records and the results are consistent with those described above. Specifically, there is a consistent increase in period of the decreasing wave B, a decrease in the growing wave A and a local minimum period coupled to the maximum of the expected wave height.

Time histories of the expected pressure variations (or pressure head variations, ζ) at transducer depths during the passage of an extreme wave group can be found from (1.3) as described above, using time series data of the measured transducer pressure and surface elevation. These are shown in figure 7. The overall similarity between this and figure 6 gives confidence in the consistency of the measurements, but there are discernible differences that can be attributed to the attenuation of the pressure signal with depth. The enhancement of wave A during its course from locations 8, 9 to location 3 is somewhat smaller than at the water surface, and this is consistent with the reduction in period of this wave during this interval. Also, the abatement of the height of wave B from point 9 to point 3 is smaller at the transducer depth (figure 7) than at the surface (figure 6) which again is consistent with the increase in period between these two points. Finally, the wave direction estimated from the pressure head wave of figure 7 is practically the same as that estimated from the surface measurements – an incidence angle of 9° instead of 11°.

3.2. *Observed extreme wave characteristics*

The highest wave ($H = 9.6\sigma$) recorded during the experiment is shown in figure 8. The same surface wave height was recorded at gauges 3 and 4 on this occasion, but the pressure head reading was higher at gauge 3. At the surface at gauge 4 the wave was

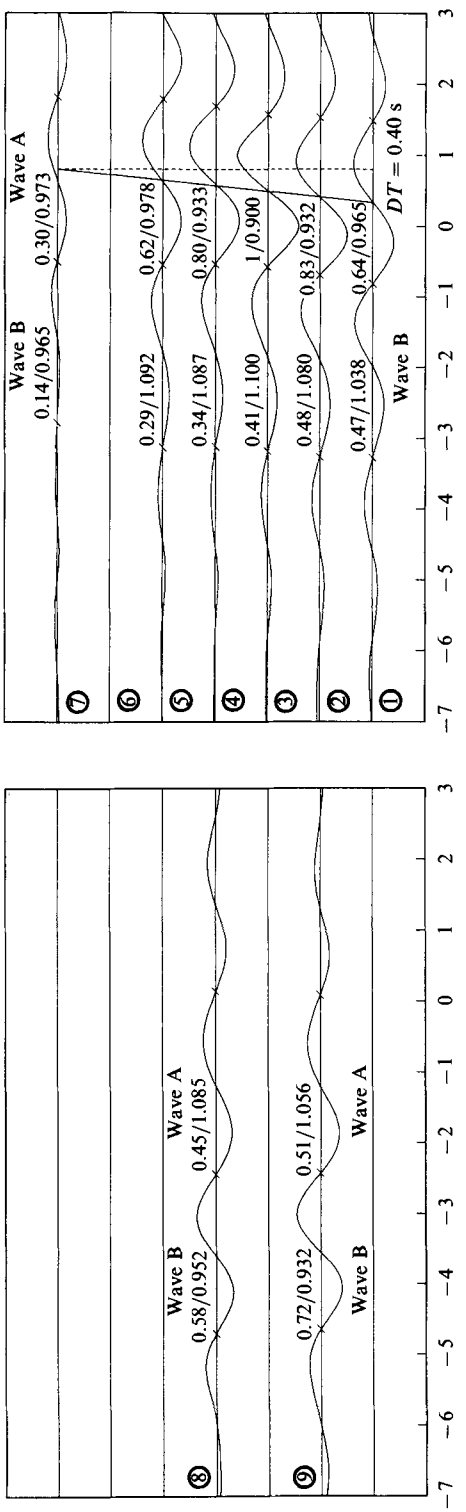

FIGURE 6. This picture was obtained from equation (1.2), using the time series data of the surface elevation of record 24, without smoothing. It shows the time histories of the expected surface waves at the locations of the gauges, if a wave with a very large height H is recorded at location 3. The first number over each wave denotes the crest-to-trough height, and the second number denotes the wave period; the wave height is scaled by given height H and the wave period is scaled by the dominant wave period T_d.

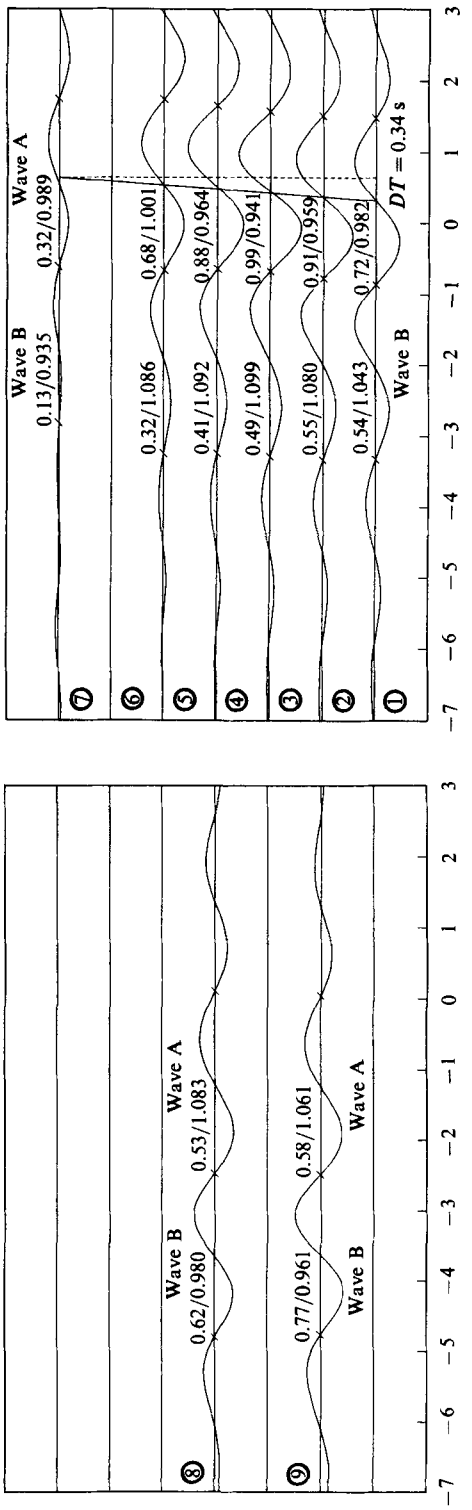

FIGURE 7. This picture was obtained from equation (1.3), using the time series data of the measured transducer pressure and surface elevation of record 24, without smoothing. It shows the time histories of the expected pressure head variations at transducer depths, if a wave with a very large height H is recorded at the surface at location 3. The wave heights are scaled to $H(\overline{\zeta^2}/\overline{\eta^2})^{\frac{1}{2}}$. The periods are scaled to the dominant period of the surface waves.

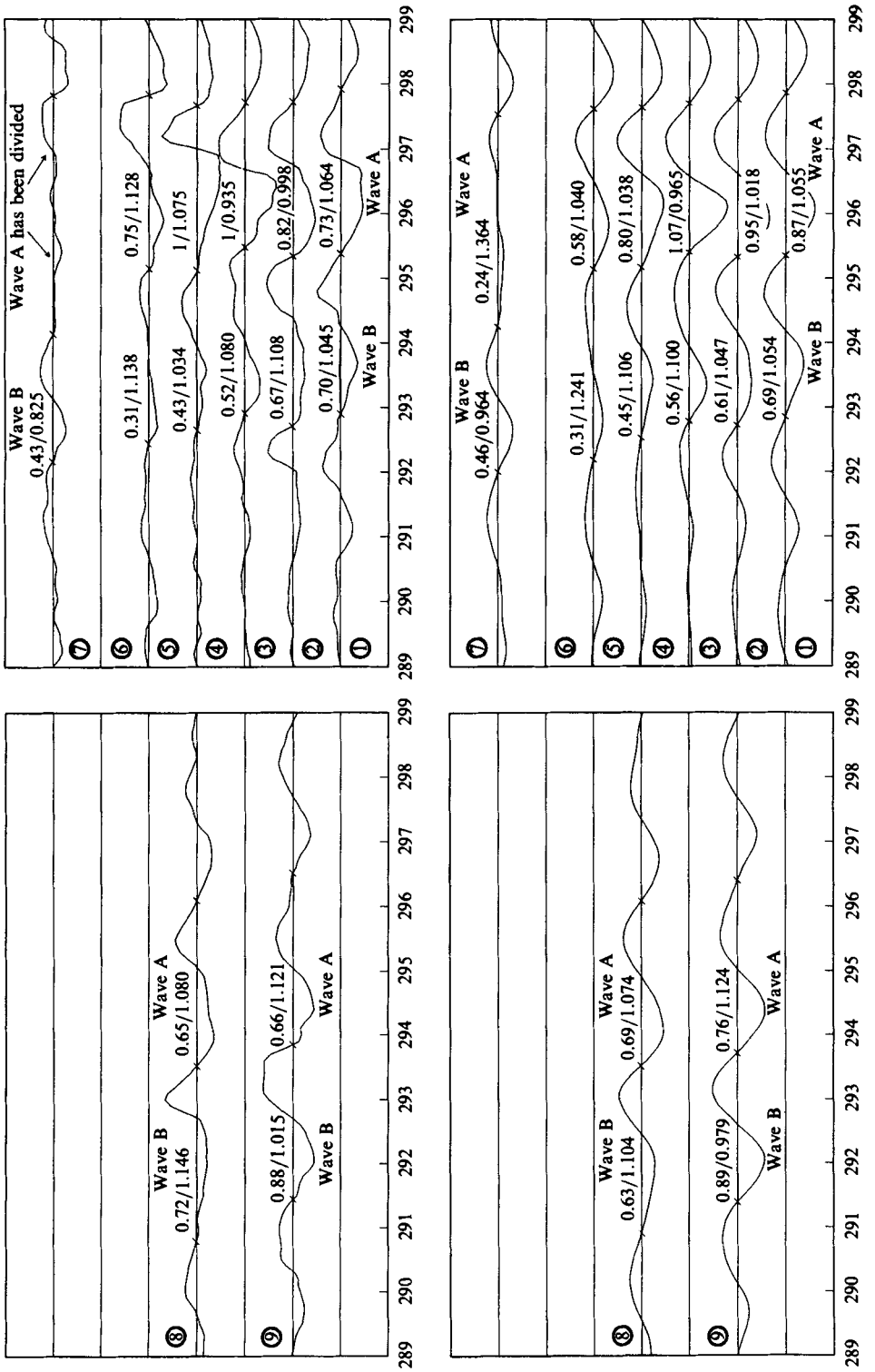

FIGURE 8. The group of the highest wave recorded during the experiment ($H = 9.6\sigma$, record 24). Upper panels: surface waves, with the heights scaled by major height H. Lower panels: pressure head waves, with the heights scaled by $H(\overline{\zeta^2}/\overline{\eta^2})^{\frac{1}{2}}$. The upper panels are to be compared with the prediction of figure 6, and the lower panels with the prediction of figure 7.

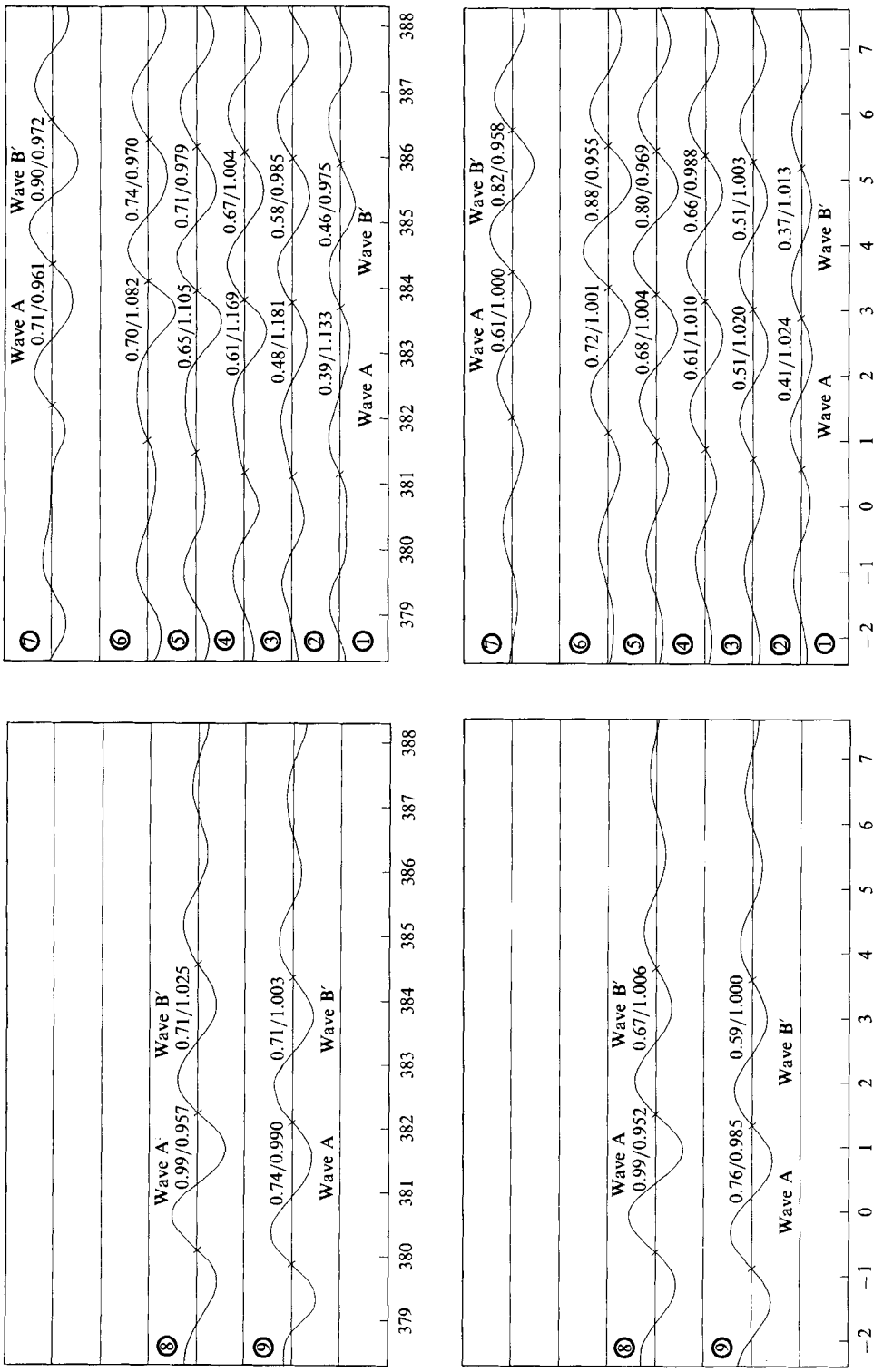

FIGURE 9. The group of the second highest wave recorded during the experiment ($H = 9.1\sigma$, record 62). Upper panels: pressure head waves recorded by the transducers. Lower panels: time histories of the expected pressure head waves calculated from equation (1.3), using the time series data of the measured transducer pressure and surface elevation of record 62.

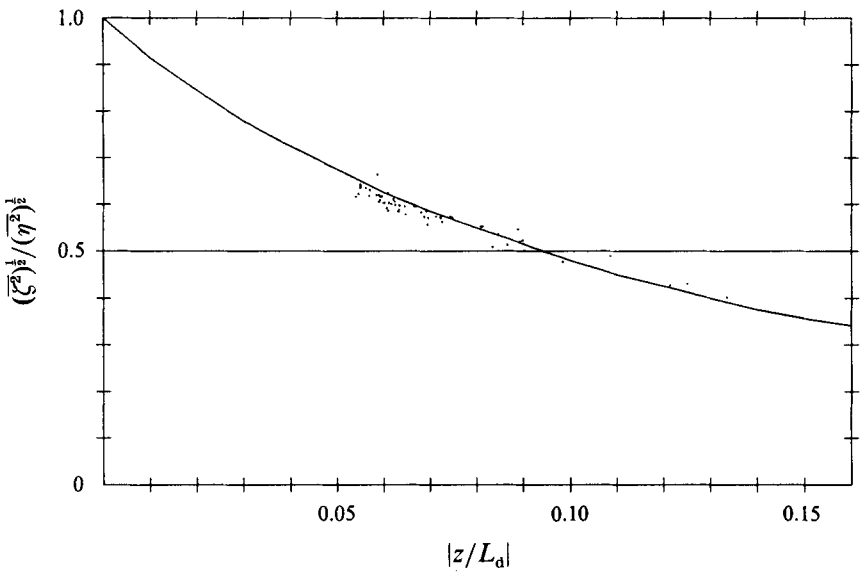

FIGURE 10. Ratio of the r.m.s. pressure head and the r.m.s. surface displacement.

sharply peaked and the associated smaller-scale pressure variations attenuate more rapidly than those for the wave as a whole. Although the records from this single realization are more irregular than the expected profiles of figures 6 and 7, the essential features described earlier are still evident, and provide good support for the theoretical connection. First, the replacement of wave B by wave A at the envelope centre occurs both in the surface wave and the pressure head waves. In particular, at the water surface, from point 9 to point 3, along the line of the energy flux, wave B decreases from $0.88H$ to $0.52H$ while A increases from $0.66H$ to H. Secondly, the period of the diminishing wave B increases both in the surface record and the pressure record, from $1.015T_d$ at point 9 to $1.080T_d$ at point 3, where T_d is the dominant overall wave period. The period of the growing wave A decreases over the same interval from $1.121T_d$ to $0.935T_d$, the local minimum period coinciding with the maximum wave height.

With reference to the quality of the measurements, we note again the agreement between the ultrasonic probes and the pressure transducers. Indeed, apart from some expected differences due to the water motion, we see that below each surface wave there is a pressure head wave with the same basic features: the trough stretching to the left in the major wave at point 4, the deeper trough and broader crest of the major wave at point 3, etc. On the crest of surface wave B at point 9, we have, on the other hand, an example of the instrumental drop-out pointed out earlier; the gauge did not receive back the reflected ultrasonic beam for a time interval of about 0.3 s and retained the output signal on the last measured wave elevation.

The second highest wave in the whole experiment was a zero up-crossing recorded at location 8. Height H of the surface wave was 9.1σ and the height of the pressure head wave at the transducer depth was $9.0(\overline{\zeta^2})^{\frac{1}{2}}$. Figure 9 shows the records of the transducers (uppers panel) and the time histories of the expected pressure head waves. These were found from equation (1.3) as described above, and the angle of incidence was estimated to be 13° – the front centre transits point 5 after point 8. We see the observed waves to reproduce the essential features of the expected waves. In particular, from locations 8, 9, to the line 1–7, wave A decreases on passing from the centre to the head of the

group while the succeeding wave B′ grows because it replaces A at the group centre. Note also the increase in period of wave A and the decrease in wave B′.

The contributions of the authors were as follows: Boccotti designed and directed the experiment, Barbaro supervised the assembly of the field laboratory, Mannino assembled and governed the instruments.

Appendix

The ratio of the r.m.s. pressure head at a fixed depth z and the r.m.s. surface displacement, for a random wind-generated sea state on deep water, is

$$(\overline{\xi^2})^{\frac{1}{2}}/(\overline{\eta^2})^{\frac{1}{2}} = \left[\int_0^\infty E(\omega)\exp\left(2\frac{\omega^2}{g}z\right)\mathrm{d}\omega \Big/ \int_0^\infty E(\omega)\,\mathrm{d}\omega\right]^{\frac{1}{2}}, \tag{A 1}$$

$E(\omega)$ being the frequency spectrum. The line in figure 10 represents ratio (A 1) as a function of z/L_{d}, for the mean JONSWAP frequency spectrum. The data points represent the values of the ratio in the 64 records. The differences between data and theory are within 7%.

REFERENCES

BOCCOTTI, P. 1988 Refraction, reflection and diffraction of irregular gravity waves. *Excerpta of the Italian Contribution to the Field of Hydraulic Engineering*, vol. 3, pp. 47–89, Padova: Libreria Progetto.

BOCCOTTI, P. 1989 On mechanics of irregular gravity waves. *Atti Accademia Nazionale dei Lincei, Memorie* VIII, **19**, 111–170.

FORRISTALL, G. Z. 1984 The distribution of measured and simulated heights as a function of spectra shape. *J. Geoph. Res.* **89**, 10547–10552.

HASSELMANN, K., BARNETT, T. P., BOUWS, E. *et al.* 1973. Measurements of wind wave growth and swell decay during the Joint North Sea Wave Project (JONSWAP), *Deut. Hydrogr. Z.* A(8) **12**, 1–95.

LONGUET-HIGGINS, M. S. 1980 On the distribution of the heights of sea waves: some effects of nonlinearity and finite band width. *J. Geoph. Res.* **85**, 1519–1523.

LONGUET-HIGGINS, M. S. 1984 Statistical properties of wave groups in a random sea state. *Phil. Trans. R. Soc. Lond.* A **312**, 219–250.

MITSUYASU, H., TASAI, F., SUHARA, T. *et al.* 1975 Observation of directional spectrum of ocean waves using a clover-leaf buoy. *J. Phys. Oceanogr.* **5**, 750–760.